Section 1
PROGRESS IN LASER FUSION

1.A Nonlinear Interactions in Long-Scale-Length Plasmas

Nonlinear laser-matter interaction processes relevant to inertial confinement fusion (ICF) have been studied experimentally and theoretically for over 25 years. During the last ten years emphasis has shifted to short-wavelength drivers ($\lambda_0 < 0.5\ \mu m$) in order to maximize collisional coupling of the laser to the corona and minimize parametric laser-plasma interaction processes both near the critical density (n_c) surface (where the laser frequency ω_0 equals the plasma frequency ω_{pe}) and at lower densities. However, as experiments approach reactor dimensions, longer gradient scale lengths will increase the likelihood of significant excitation of these processes. To the extent that these processes involve the generation of plasma waves, they are potential sources of energetic electrons that could prevent efficient compression of the fuel. It is therefore important to continue to investigate these processes and their scaling laws under conditions approaching those of future larger-scale experiments. In particular, it is important to investigate the impact that beam-smoothing schemes have on these nonlinear processes.

In this article we will discuss a series of experiments on nonlinear interaction processes carried out on long-scale-length laser plasmas produced with the 24-beam OMEGA laser system. We will also offer our present understanding and interpretation of these experiments, although some of the suggestions are still rather tentative. The main processes considered are the two-plasmon decay (TPD) instability as evidenced by its traditional signature, the 3/2-harmonic emission from the plasma, and Raman scattering at densities below quarter critical.

Experimental Conditions

The background plasma for these experiments is furnished by first exploding mass-limited CH targets (0.6-mm diam, 6-μm thick) with eight primary beams.[1] This is followed by irradiation with eight secondary beams, delayed 0.6 ns relative to the primaries, which maintain the electron temperature $T_e > 1$ keV over a period of ~0.5 ns. Each laser beam has an energy of ~50 J at a vacuum wavelength of $\lambda_0 = 351$ nm, and the pulse duration is 0.6 ns. Furthermore, all beams are outfitted with distributed phase plates[2,3] (DPP's) of 1.25-mm-diam hexagonal cell size yielding a minimum spot diameter of 380 μm (the first zero of the Airy pattern). These beams are strongly defocused (FWHM ≈ 450 μm) in order to irradiate the target as uniformly as possible at intensities $\leq 5 \times 10^{13}$ W/cm^2. Occasionally four to six tertiary beams have also been employed; these beams are delayed by 1 ns relative to the primaries, and their wavelength is 1.054 μm for increased absorption at late times. The production and characterization of the background plasma has been described extensively in Ref. 1.

This plasma is then irradiated by an interaction beam, also at $\lambda_0 = 351$ nm, with energy up to 60 J and a pulse duration also of 0.6 ns. The diameter of the DPP cells is increased by a factor of 2 for the interaction beam in order to obtain a maximum average interaction-beam intensity on target of ~10^{15} W/cm^2. (This is the peak intensity in space and time of the envelope of the target-plane profile.) Some of the experiments were carried out with the addition of FM bandwidth ($f_{FM} = 10$ GHz, $\Delta\lambda/\lambda \leq 3 \times 10^{-4}$) and appropriate angular dispersion on all beams, resulting in beam smoothing by spectral dispersion[4] (SSD). The primary diagnostics for these experiments were visible and UV spectroscopy, with and without time resolution. The directions of observations were chosen to optimize either the 3/2-harmonic emission (in the plane of polarization and at 20° from the backscatter direction) or the Raman signal (out-of-plane at 45° to the backscatter direction or direct backscatter).

Three-Halves Harmonic Spectra

The spectrum of this emission is always characterized by two peaks, usually asymmetrically displaced relative to $3\omega_0/2$, with the red-shifted component usually the stronger one. This signature is commonly attributed to Thomson (or Raman) scattering of interaction-beam photons off plasmons produced by the same beam through the TPD instability.[5,6] We will call this process "self-scattering." In fact, the first observations of this instability were through its characteristic 3/2-harmonic emission.[7] Various theories[8] have since been proposed to precisely relate the TPD plasmons to the observed spectral features. However, none of these theories have been very successful[9] and a generally accepted explanation of these features is still forthcoming.

The current experiments differ from previous ones in that we are able to change experimental conditions to highlight different features of the 3/2-harmonic spectra. Time resolution of these spectra has been found to be indispensable. Typical spectra for four different experimental conditions are shown in Fig. 51.1. Most features in Figs. 51.1(b)–51.1(e) are caused by the self-scattering, either from the primary beams [the weak signals on the left of

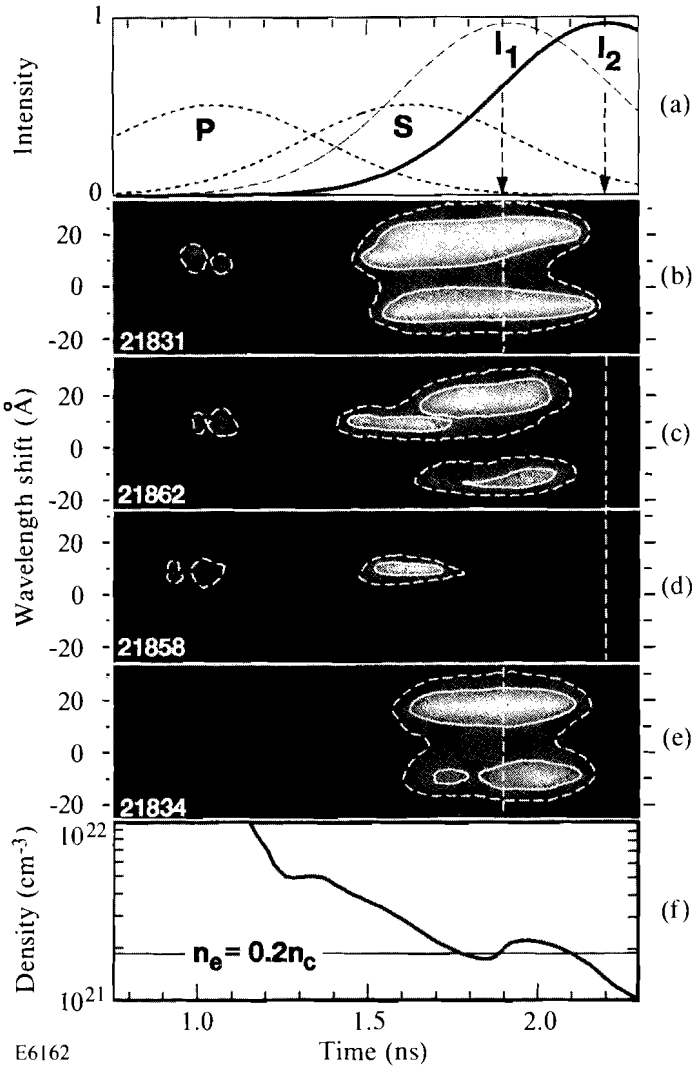

Fig. 51.1
Typical sequencing of the primary, secondary, and interaction beams (a), and time-resolved 3/2-harmonic spectra for different timings of the interaction beam: (b) 1.9 ns (I_1), (c) 2.2 ns (I_2), (d) 2.2 ns (I_2), and (e) 1.9 ns (I_1). Shots (b) through (d) had no FM bandwidth, while (e) had an SSD bandwidth of $\Delta\lambda/\lambda \approx 3 \times 10^{-4}$. In (f) the time evolution of the peak on-axis density calculated by *SAGE* (for primary and secondary beams only) is shown with the TPD Landau cutoff indicated at $n_e = 0.2\ n_c$. The interaction-beam intensity is ~10^{15} W/cm^2 for all figures but (d), for which it is ~2×10^{14} W/cm^2. The primary and secondary beam intensities are ~5×10^{13} W/cm^2. The wavelength of all beams is 351 nm. In (c) an additional six tertiary beams of $\lambda = 1054$ nm were added, with their peaks at 2 ns. The contour lines shown correspond roughly to the 50% and 20% of maximum intensity.

Figs. 51.1(b)–51.1(d), near t ≈ 1 ns], or from the interaction beam (the strong, double-lobed signals on the right). In addition, an unusual red-shifted spectral component, which starts around 1.5 ns and lasts until about 1.7 ns, is observed in Figs. 51.1(b)–51.1(d). It is most easily seen in Figs. 51.1(c) and 51.1(d). In Fig. 51.1(d) this is the only feature related to the interaction beam since the interaction beam intensity was reduced to below the threshold for self-scattering, 3/2-harmonic generation. This signal disappears if either the secondary beams or the interaction beam is turned off. We have identified this red-shifted spectral component (hereafter referred to as the "probe-beam" feature) as being a result of Thomson scattering involving plasmons from the TPD instability of one of the secondary heating beams (OMEGA beam 32) and probe-beam photons from the interaction beam. A discussion of these two distinctive 3/2-harmonic features follows.

1. Probe-Beam Feature

The experimental geometry permitting observation of this spectral feature is shown schematically in Fig. 51.2 with the location of the interaction beam on the equator of the target chamber (east), the 3/2-harmonic observation port ~20° above (north) and in the plane of polarization of the interaction beam, and the secondary beam 32 located northeast at 50° latitude with its polarization pointing half-way between the interaction beam and the observation port. Beam 32 is the only one of the secondary beams that can produce "red" TPD plasmons with k-vectors that point roughly half-way between the interaction beam port and the 3/2-harmonic observation port. Furthermore, these plasmon k-vectors have the right length for 3/2-harmonic generation using a photon of the interaction beam. The corresponding k-vector diagrams are shown schematically in the boxes in Fig. 51.2. From calculations we find that these red plasmon k-vectors have $k_{p,r} \approx 2k_{o,vac}$, where $k_{o,vac}$ is the vacuum propagation vector of the λ_o = 351-nm laser beam producing the TPD instability. The geometry and electron temperature determine uniquely the electron density at which the TPD occurs and the wavelength shift of this probe-beam feature relative to $2\lambda_o/3$.

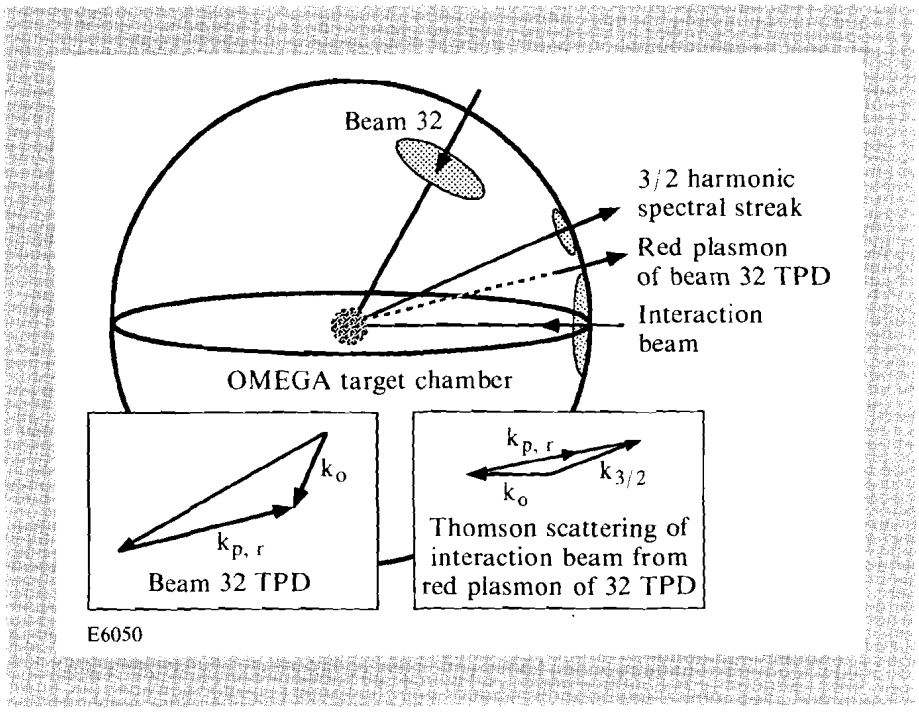

Fig. 51.2
Schematic scattering diagram for probe-beam feature of 3/2-harmonic emission. Top part refers to target-chamber geometry; boxes show two-step scattering process for TPD decay of beam 32 and subsequent Thomson scattering involving the interaction beam. The vector $k_{3/2}$ points toward the observation port.

The density at which the corresponding TPD instability takes place is given by

$$n_e / n_c \approx 0.25\left(1 + 3\kappa^2 \lambda_D{}^2\right)^{-1}, \tag{1}$$

and the corresponding red shift of the probe-beam feature $\Delta\lambda_{3/2}$ can be calculated from

$$\Delta\lambda_{3/2} / \lambda_{3/2} \approx 0.5(k_o \lambda_D)(\kappa\lambda_D)\cos\theta / \left(1 + 3\kappa^2\lambda_D^2\right), \tag{2}$$

where $\kappa = k_o/2\text{-}k_{p,r}$ and $\cos\theta = \kappa \cdot k_o/(\kappa\, k_o) \approx 0.66$ are determined by the experimental geometry (Fig. 51.2). The electron Debye length is denoted by λ_D. Using $T_e \approx 1$ keV and κ as determined geometrically, we obtain from Eq. (1) $n_e \approx 0.23\ n_c$, which is well above the Landau cutoff density of $0.2\ n_c$ (see the following), and from Eq. (2) $\Delta\lambda_{3/2} \approx 12$ Å. This calculated wavelength shift agrees very well with the 10 Å to 11 Å measured in our experiments. The angle $\theta \approx 49°$ is also very close to the optimum angle for the growth of the TPD instability.[6]

The probe-beam feature can be used advantageously to determine the TPD threshold during the falling part of the secondary heating beam (beam 32). The interaction beam, which acts here merely as a "probe" beam, increases steadily during the same period so that the disappearance of the Thomson signal corresponds to the disappearance of the TPD instability at that density. We can use this cutoff to obtain an upper limit to the experimental TPD threshold of $2\text{–}3 \times 10^{13}$ W/cm^2. This is approximately a factor of 2 below the usual linear gradient threshold[10] of $\sim 5 \times 10^{13}$ W/cm^2. The instability could disappear either because the intensity of the secondary beam falls below the TPD threshold or because the plasma density falls below $0.23\ n_c$. If the background density had actually fallen below $0.23\ n_c$, our experimental threshold would clearly be an overestimate. The difference between the experimental and calculated thresholds may be a result of filamentation of beam 32 in the plasma, for which Epperlein[11] has estimated a threshold of $\sim 10^{13}$ W/cm^2. In contrast, use of the self-scattering threshold (the onset of the main 3/2-harmonic, double-lobed feature caused by the interaction beam in Fig. 51.1) would result in an inferred TPD threshold that is ten times higher than the probe-beam estimate given previously! The reason for this higher threshold lies in the complexity of the self-scattering signal, as will be discussed. Note that we do not see any evidence of self-scattering, 3/2-harmonic emission from the secondary heating beams alone.

2. Self-Scattering Feature

The main spectral features of the 3/2-harmonic emission are caused by self-scattering, with the interaction beam creating the TPD plasmons and then scattering off these plasmons. The measured spectral splitting of this feature is ~28 Å, with the red component shifted by ~+16 Å relative to $2\lambda_o/3$ and the blue component shifted by ~−12 Å. In addition, the red component is usually stronger than the blue component.

In principle, for high intensities the TPD instability should extend all the way to the Landau cutoff at $k_p\lambda_D \approx 0.3$, and indeed we require this to explain our experimental observations.[12] We can use Eq. (1) with $\kappa\lambda_D = 0.3$ to estimate the Landau cutoff density and obtain $n_e \approx 0.2\ n_c$. The magnitude of each of the TPD plasma-wave k-vectors at this density is $\sim 3k_{o,\mathrm{vac}}$. Ignoring the details of the scattering process leading to the self-scattering, 3/2-harmonic emission, one can obtain a splitting of the 3/2-harmonic spectrum by equating it to the frequency difference between the two TPD plasmons at the Landau cutoff. The corresponding wavelength shifts for the red and blue 3/2-harmonic spectral components are obtained from Eq. (2), using $\kappa\lambda_D = 0.3$ and $\theta \approx 45°$, resulting in $\Delta\lambda_{3/2} \approx 17$ Å. This is in good agreement with the position of the red peak; but, as noted

previously, the shift of the blue peak is only about 12 Å. This smaller shift of the blue peak will be discussed further. Since the self-scattering, 3/2-harmonic spectra show a clear double-peak structure with little emission between the peaks, we conclude that this feature originates predominantly from the region near 0.2 n_c, with little or no contribution from the TPD at higher densities.

A more fundamental problem is that the wave-vector matching conditions do not permit the combination of a laser photon with wave vector k_0 with a plasmon of wave vector $\sim 3k_0$ to produce a $3\omega_0/2$ photon with wave vector $\sim 3k_0/2$. One possible solution is to invoke weak turbulence: the plasmons decay repeatedly into ion-acoustic phonons and plasmons of shorter wave vector; after sufficient steps in this cascade their wave vectors are short enough to satisfy the matching conditions for $3\omega_0/2$ emission. Unfortunately, the cascade also reduces the frequencies of the plasmons, resulting in the average wavelength of the two $3\omega_0/2$ photons being shifted to the red by ~15 Å. This is much larger than the observed asymmetry and this explanation can therefore be ruled out.

Locally steep density gradients provide a means of relaxing the wave-vector matching conditions without changing the plasmon frequencies, since in steep gradients the wave vectors no longer have a precise value. One potential source of such gradients is strong turbulence, in which the plasmons become trapped in collapsing cavitons[13] near $n_e \approx 0.2\ n_c$. This model also accounts for the higher threshold of the self-scattering, 3/2-harmonic emission compared with the TPD instability since the energy density of the TPD plasma waves must rise to $\sim (k_p \lambda_D)^2\, n_e k_B T_e$ before strong turbulence sets in. However, since the threshold for strong turbulence is lower for smaller plasmon wave vectors, and therefore at higher densities, this model does not explain why most of the self-scattering, 3/2-harmonic emission occurs at the Landau cutoff density, nor does it account for the asymmetry of the spectrum.

Another possibility is a sharp density gradient localized at the Landau cutoff density. Such a gradient could result from the rapid drop in plasmon ponderomotive pressure near the cutoff;[14,15] the rapid drop in effective pressure would drive an increase in flow velocity and concomitant decrease in density near the cutoff. Besides explaining the preponderance of emission at the Landau cutoff, this model also naturally accounts for the asymmetry of the two peaks in wavelength and intensity: since the blue (higher-frequency) plasmons created by the TPD instability propagate *into* the plasma, they must undergo one ion-acoustic decay to reflect them back toward the cutoff. The frequency decrease ($2k_{p,b}c_s$) resulting from this decay is calculated to produce a wavelength shift of ~6 Å to the red for the resulting $3\omega_0/2$ light. Thus, the wavelength shift for the blue peak is reduced to ~11 Å, in good agreement with observation. The red plasmons, on the other hand, are created propagating outward and need undergo no reflection to reach the cutoff; thus the red peak remains shifted by 17 Å and retains its full intensity.

3. Influence of Beam-Smoothing Techniques on the 3/2-Harmonic Spectra

Figure 51.1(e) is an example of a time-resolved, 3/2-harmonic spectrum in the presence of SSD, which combines distributed phase plates, FM bandwidth, and angular dispersion. We note that the weak emission at the time of the primary

beams has disappeared as has the probe-beam feature around 1.5 ns. This implies that the TPD threshold as estimated from the probe-beam feature must have increased in these experiments by at least a factor of 2. Unfortunately, no data with variable intensity in beam 32 are currently available to establish a clear threshold. However, judging from intensity measurements made on time-integrated, self-scattering spectra using the interaction beam, we do not think that the threshold has increased by much more than a factor of 2. This can also be deduced—albeit with less accuracy—from the time-resolved data in Figs. 51.1(b) and 51.1(e). Doubling our original TPD threshold estimate based on the probe-beam feature brings it in very close agreement with the gradient threshold assuming 500-μm gradient scale lengths. (The theory for the TPD threshold in a parabolic density profile is not available at this time.)

At present we speculate that filamentation,[11] without SSD, sets in around 10^{13} W/cm^2. The enhanced intensity inside the filaments then reduces the apparent TPD threshold from that in the background plasma. Hydrodynamic arguments along with the optics of SSD suggest that a 10-GHz FM modulation with a bandwidth of $\Delta\lambda/\lambda \sim 3 \times 10^{-4}$ is sufficient to significantly reduce if not completely eliminate filamentation. Since the TPD threshold is not far above the filamentation threshold, the influence of filamentation on the overall TPD instability level well above threshold may not be very noticeable.

This speculation is supported by direct experimental evidence for filamentation found by Coe *et al.* in long-scale-length plasmas,[16] and by indirect evidence in the same plasmas through stimulated Raman and Brillouin scattering by Willi *et al.*[17] Using the same experimental techniques, this group reported both direct and indirect evidence for the suppression of filamentation when beam-smoothing techniques, such as induced spatial incoherence (ISI), were applied.[18,19]

Peyser *et al.*[20] have reported significant reduction of 3/2-harmonic emission from laser plasmas when ISI beam-smoothing techniques were used. They have noted a fivefold increase in the TPD threshold for bandwidths of 5 Å to 10 Å at an interaction wavelength of 527 nm. They have attributed these observations partly to the suppression of filamentation and partly to direct bandwidth effects on the instability growth rates. However, in these experiments the same beam was used as the interaction beam and the plasma-producing beam, thus complicating the interpretation, since the plasma conditions change as the irradiation intensity changes. While we agree with their interpretation concerning suppression of filamentation, we see no evidence in our experimental results that the modest bandwidths applied in our case have any direct influence on reducing the 3/2-harmonic emission.

Further support for our filamentation hypothesis has been provided by two- and three-dimensional (2-D and 3-D) simulations by Schmitt,[21] which clearly demonstrate the effect of ISI-type beam-smoothing techniques on the reduction or suppression of filamentation.

In all time-resolved, 3/2-harmonic spectra we note that the spectra end abruptly near 2.1 ns, independent of whether the interaction beam peaked

before or after this time (see Fig. 51.1). Comparing this observation with Fig. 51.1(f) we note that this corresponds to the time when the predicted peak on-axis density dips below 0.2 n_c, the TPD Landau cutoff density. (The predictions for this time are insensitive to the timing of the interaction beam.) This may be taken as a confirmation of the interpretation that the self-scattering, 3/2-harmonic emission involves TPD decay near the Landau limit, i.e., at densities much closer to 0.2 n_c than 0.25 n_c. Conversely, this observation is a confirmation of the predictive capability of the 2-D hydrodynamic code *SAGE*.

There is a further point of interest: the dip in the 3/2-harmonic emission near 1.8 ns, best observed in Fig. 51.1(e), corresponds very well with the excursion of the peak on-axis density below 0.2 n_c at the same time as predicted by *SAGE* and shown in Fig. 51.1(f). (The increase in the on-axis density at 2.0 ns is a result of mass flow toward the axis from the less-well-irradiated off-axis portion of the foil and is discussed in detail in Ref. 1.) The dip in the 3/2-harmonic emission is better seen in the blue component than in the much more intense red component, for which the streak record was very close to or beyond the saturation level. In the streaks without SSD this modulation may be washed out, either because of the generally high signal levels of the streak records or by complex interactions involving filamentation of the strongly modulated, stationary intensity distribution (speckle pattern). It should also be noted that this dip in density could affect our estimates of the TPD threshold on the basis of the probe-beam feature as was noted previously.

Amiranoff *et al.*[22] and Basov *et al.*[23] have carried out 0.53-μm probe-beam experiments using solid targets irradiated at 1.064 μm at an intensity of ~10^{15} W/cm^2. They were able to probe plasmons with k-vectors very close to the TPD Landau cutoff. While refraction of the various waves is certainly a significant problem for the interpretation of all of these experiments, Basov *et al.*[23] were able to deduce spectra of the plasma turbulence near $n_c/4$, which clearly extended to the Landau cutoff. Their results also indicated a drop in the turbulent plasma wave spectrum for $k_p\lambda_D \leq 0.13$, which the authors ascribe to density-scale-length effects. These probe-beam experiments are similar to the probe-beam experiments presented here, but they are relevant to the self-scattering regime because of the high intensities in the interaction beam. They also support our conclusions that the TPD instability extends all the way to its Landau cutoff.

Raman Spectrum

Raman scattering has been observed in many high-intensity, laser-produced plasmas.[17, 24–27] The data presented here are both time integrated and time resolved and agree in many respects with observations elsewhere. However, on a number of points we come to significantly different conclusions, based on the combination of our Raman and 3/2-harmonic data and the data presented in Ref. 1.

Typical time-integrated Raman spectra are shown in Fig. 51.3 for the interaction beam peak timed at 1.6 and 2.2 ns. Compared with the spectra reported by Drake *et al.*,[25] these spectra are very narrow in spite of the fact that the interaction beam intensities are nominally comparable. The narrowness of

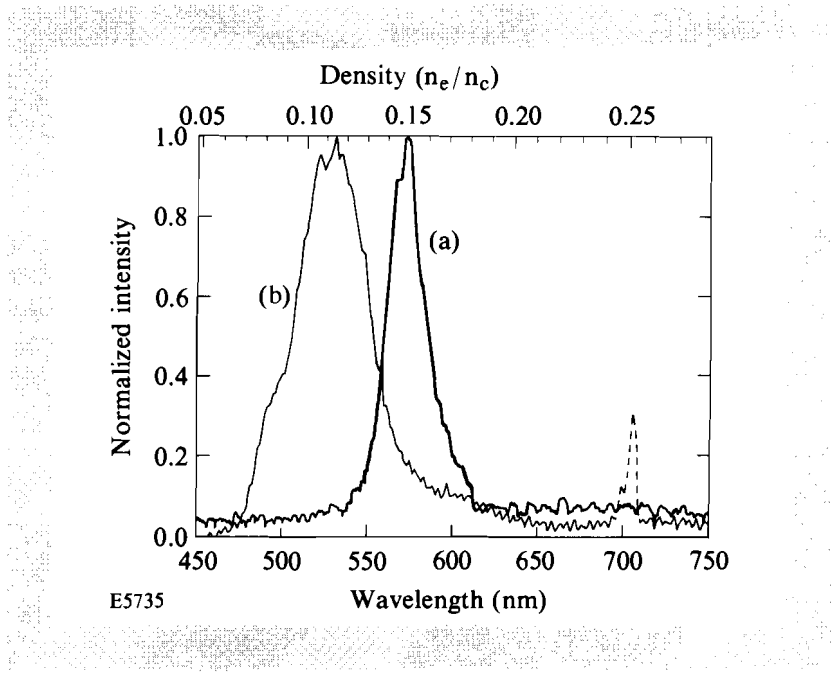

Fig. 51.3
Typical time-integrated Raman spectra obtained for two different timings of the interaction beam: (a) t = 1.6 ns, (b) t = 2.2 ns. Note: the 700-nm feature drawn dashed in (b) is caused by 3/2-harmonic emission from the 1054-nm tertiary heating beams that were on for this shot. (Any 1/2-harmonic emission from the 351-nm beams is fully reabsorbed by the plasma.)

our data indicates that the emission occurs over a small density range (see top scale in Fig. 51.3). In Ref. 1 we interpreted this as an indication that the Raman emission emanates from the maximum of the on-axis density profile, which is relatively stagnant around 1.6 ns while it decreases with time rather rapidly around 2.2 ns, in agreement with the wider Raman spectrum for this case.

The intensity dependence of the Raman emission at 45° to the backscatter direction shows a clear threshold near 2×10^{14} W/cm^2 with a linear growth region extending over nearly four orders of magnitude (see Fig. 51.4). Saturation appears to set in at an intensity only four times higher than the threshold. These data were all taken with the interaction beam peaking at 1.6 ns with all spectra closely resembling that of Fig. 51.3(a). The observed SRS threshold is actually very close to the collisional SRS threshold $I_{\text{Raman,coll}}$ in a parabolic density profile given by Williams[28] as

$$I_{\text{Raman,coll}} \approx 2.5\times10^{16} Z^{1/2}\left(n_e/n_c\right)^{1/4} / \left(T_{\text{keV}}^{3/2}\,\lambda_\mu^{3/2}\,L_\mu\right) \text{W/cm}^2 \ , \quad (3)$$

where Z is the average ionic charge, λ_μ is the laser wavelength in microns, and L_μ is the FWHM of the parabolic density profile $n_e/n_c = 1–2\ (x/L_\mu)^2$. For our experiments, with a typical value of $L_\mu \approx 500$ μm, Eq. (3) yields $I_{\text{Raman,coll}} \approx 2.5\times10^{14}$ W/cm^2.

Three typical time-resolved Raman spectra are shown in Figs. 51.5(a)–51.5(c) displayed on a common time axis with the interaction beam ($I_0 \sim 10^{15}$ W/cm^2) peaking at 2.0, 2.4, and 2.6 ns, respectively. The background plasma was created in the same way in all cases, but the electron temperature evolution is expected to be different because of more (and earlier) heating caused by the interaction beam in the first case.[1] In all cases the Raman emission occurs early

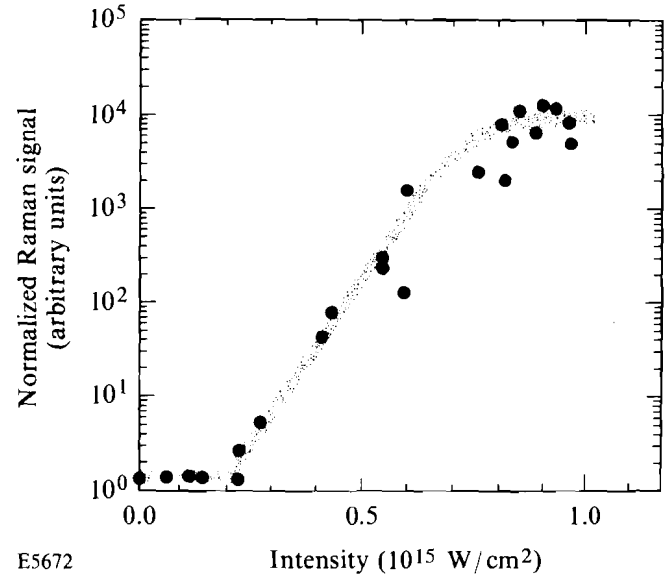

Fig. 51.4
Intensity dependence of the Raman emission for the peak of the interaction beam at $t = 1.6$ ns. These experiments used distributed phase plates on all beams but no applied FM bandwidth (no SSD).

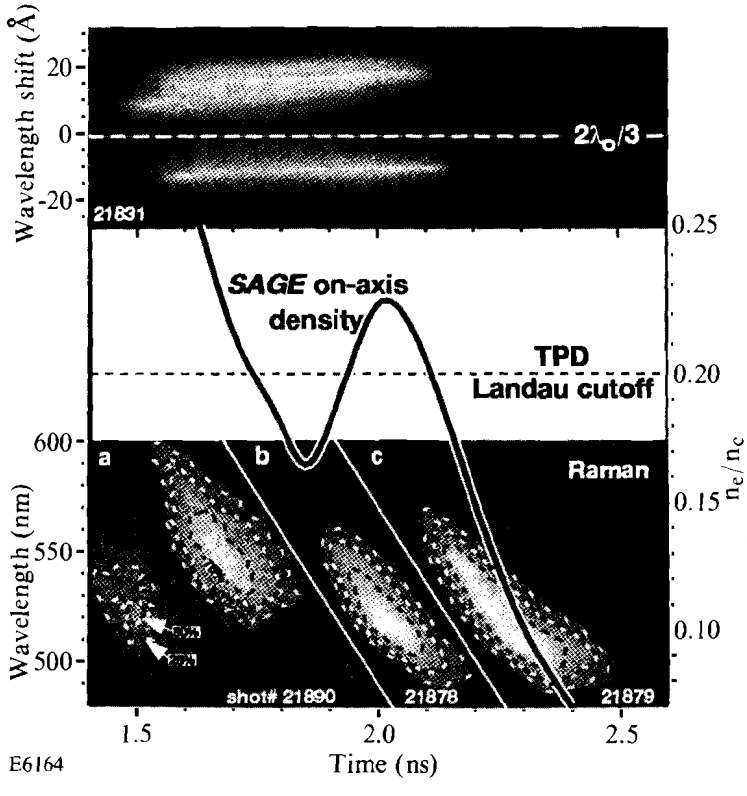

Fig. 51.5
Time-resolved Raman spectra for three shots without SSD and with the interaction beam of intensity ~10^{15} W/cm^2 peaking at (a) 2 ns, (b) 2.4 ns, and (c) 2.6 ns. Tertiary heating beams were present in (a) but in none of the other shots. There is no additional structure beyond the straight white lines separating the different shots. Superposed on the streaks is the peak on-axis density evolution as calculated by *SAGE* in the absence of the interaction beam. The Landau cutoff (the late-time, short-wavelength cutoff) is indicative of the electron temperature $T_{keV} \approx 10\, n_e/n_c$. A typical 3/2-harmonic streak for an interaction beam with its peak at 1.9 ns [see Fig. 51.1(b)] is shown on top for comparison.

during the interaction beam and ends well before its peak. Furthermore, the emission is observed at Raman wavelengths corresponding to densities well below 0.2 n_c. It should be noted that Raman emission at $\lambda \geq 640$ nm (corresponding to emission at $n_e/n_c \geq 0.2$) typically suffers more than 75% absorption while propagating out through the plasma, whereas absorption below 550 nm is basically negligible. Observation of Raman emission from densities >0.2 n_c is therefore unlikely. On the other hand, if the actual Raman emission (i.e., the emission before propagation through the plasma) had peaked above 640 nm, we should have seen more evidence for it, either in the time-resolved spectra taken at 45° or in the time-integrated spectra taken simultaneously at 0° (backscatter). We therefore conclude that the Raman emission occurred primarily at densities <0.2 n_c. This is consistent with numerous earlier experimental observations of what is often referred to as the "Raman gap" (little Raman signal between ~0.2 n_c and 0.25 n_c). There is no generally accepted explanation for this gap.

Comparing the time-resolved Raman spectrum in Fig. 51.5(c) with the peak density evolution obtained from the simulations [dotted curve of Fig. 7(b) of Ref. 1, also shown in Fig. 51.5], we find reasonable agreement between the two. The peak of the interaction beam (~10^{15} W/cm^2) for this shot was very late, at 2.6 ns, at which time it is absorbed very weakly by the plasma. From Ref. 1 the perturbation to the plasma density profile caused by this interaction beam should be negligible. This spectrum suggests that the Raman emission shown in Fig. 51.5(c) originates from the peak of the density profile with the onset corresponding to the collisional threshold obtained from Eq. (3). The difference in detail (~20%) between the densities as determined from the Raman emission and predicted by *SAGE* is well within the predictive capability of such simulations and the less-than-perfect symmetry obtainable experimentally. Similar arguments probably account for the 3/2-harmonic emission near 1.9 ns not ceasing as expected (the predicted density dips below 0.2 n_c), although shots with beam smoothing show some indications of the existence of this dip [Fig. 51.1(e)].

The short-wavelength (low-density) cutoff observed at later times is consistent with Landau damping of the Raman plasma waves. This cutoff wavelength can be used as a temperature diagnostic;[29,30] from $k_p\lambda_D \approx 0.3$ and the dispersion relations we find $T_{\text{keV}} \approx 10\, n_e/n_c$ for cutoff densities near or below 0.1 n_c. The temperature thus determined (~1 keV at $n_e/n_c \approx 0.08$) is consistent with the temperatures found in Fig. 7 of Ref. 1 at 2.3 to 2.5 ns.

In contrast, the temporal evolution of the Raman spectra shown in Fig. 51.5(a) and 51.5(b) does not agree so well with the predicted evolution of the peak density. For these shots the interaction beam peaked at 2.0 and 2.4 ns, respectively. The narrowness of the instantaneous Raman spectra indicates that, instantaneously, most of the emission occurs in a very narrow density region that rapidly decreases toward lower densities down to the Raman Landau cutoff. In Fig. 51.5(a) the temperature inferred from the Raman Landau cutoff (~1.3 keV at $n_e/n_c \approx 0.13$) is a little higher than that in Fig. 51.5(c), again consistent with the simulations showing higher temperatures at earlier times.

At present there is no very convincing explanation for the observed temporal evolution of the Raman spectra at early times, when the peak density is >0.2 n_c

as expected from simulations and apparently confirmed by the 3/2-harmonic spectra shown in Fig. 51.1 and on top of Fig. 51.5. The observed temporal evolution of these Raman spectra indicates that the emission takes place at a density that decreases much more rapidly than the peak density in the hydrodynamic simulations. The calculated density history with the interaction beam at 2.0 ns [as for Fig. 51.5(a)] is slightly lower than the solid curve of Fig. 51.5, but not enough to match the Raman emission of Fig. 51.5(a). It is possible that the code may underestimate the extent to which the interaction beam perturbs the preformed plasma. With a 2-D density profile that has a minimum on axis (such as happens up to ~1.8 ns according to Fig. 12 of Ref. 1) one could obtain simultaneous Raman emission at 0.15 n_c from the axis and $3\omega/2$ emission at 0.20 to 0.25 n_c off-axis, with both emissions coming from the central portion of the plasma. However, a number of alternative explanations should also be considered, such as filamentation or self-focusing, profile steepening near 0.2 n_c, or the bump-on-tail instability. Direct evidence of Raman scattering from filaments has been reported by Willi *et al.*[19] and indirect evidence has been widely reported.[17,18,31,32] Alternatively, profile steepening[14,15] in the vicinity of the TPD Landau cutoff at 0.2 n_c, with the drop increasing in time, could also account for our observed Raman spectra. Finally, similar spectra could be explained by enhanced Thomson scattering[33] driven by pulses of fast electrons that excite bump-on-tail plasmons. These electrons would have their origin in the vigorous TPD instability above 0.2 n_c, and the fall of Raman wavelength in time would be explained by a decrease in directed energy of the fast-electron pulses as the plasma length increases. One should also note the interesting feature in the bottom-left portion of Fig. 51.5(a), corresponding to Raman emission from a low density at an early time. Similar features have been seen on other streaked spectra taken during the early phases of the expanding plasma.

Independent of the model used, the simultaneous emission of the 3/2 harmonic (TPD at densities $\gtrsim 0.2\, n_c$) and Raman scattering from densities below 0.2 n_c clearly indicates that the long-wavelength cutoff of the Raman spectra does not necessarily provide a reliable measure of the peak on-axis density evolution. This is in marked contrast to the general understanding that Raman spectra can be used as diagnostics of the peak density.[17,25,34]

It should also be noted that the onset of the Raman spectra coincides with the onset of the TPD self-scattering signal, which may indicate a relationship between the two processes. Such a relationship has been postulated previously by Simon and Short.[33,35] The strongly driven TPD instability leads to caviton collapse and the generation of pulses of fast electrons. The observed Raman spectra could then be a result of enhanced Raman scattering from plasma waves created lower in the density gradient by these electrons. However, this model would not apply to the Raman emission of Fig. 51.5(c) that occurs at times (>2.1 ns) beyond which no 3/2-harmonic emission is seen (Fig. 51.1) and for which *SAGE* predicts peak densities <0.2 n_c.

The sensitivity of the Raman emission to the SSD beam-smoothing technique is shown in Fig. 51.6, where a modest bandwidth of $\Delta\lambda/\lambda = 3 \times 10^{-4}$ is shown to

lead to a reduction in the Raman signal by three orders of magnitude. A similarly dramatic reduction in Raman scattering was observed by Obenschain *et al.*[31] in $\lambda = 1.054$-μm, solid-target irradiation experiments using ISI ($\Delta\lambda/\lambda = 1.5 \times 10^{-3}$). However, a detailed comparison of these experiments with our results is difficult because of the very different nature of the plasma, very different scale lengths, and different irradiation wavelengths. In long-scale-length, 527-nm-irradiation experiments at Rutherford, Willi *et al.*[19] have also observed significantly reduced Raman emission, although less dramatic than in the experiments reported here. Unfortunately, their irradiation intensities were limited to values below the SRS threshold in the presence of ISI. In both of these reports it was noted that reduction or suppression of filamentation caused by the ISI beam-smoothing technique is likely the primary reason for the reduced SRS signal strengths, rather than direct reduction of the SRS growth rates[36] caused by the applied bandwidth. Similarly, any modification of the collapse process by SSD might also decrease the hot-electron emission and thus decrease any enhanced Raman scattering.

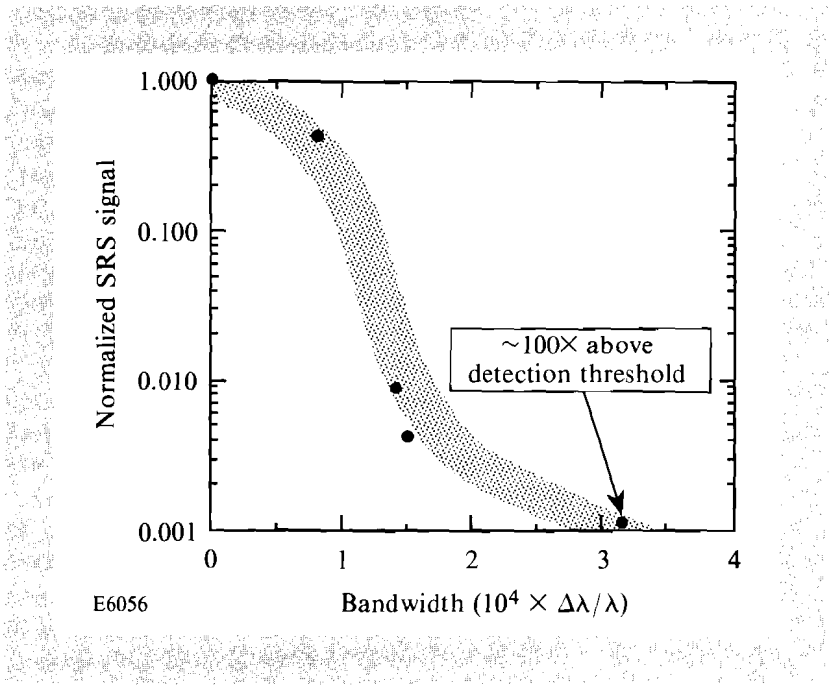

Fig. 51.6
Dependence of Raman signal on applied FM bandwidth for smoothing by spectral dispersion (SSD). The interaction-beam intensity is ~10^{15} W/cm^2 and its peak is at 1.6 ns. The background plasma conditions are the same as for Fig. 51.4.

Alternatively, only a small increase in the Raman threshold (by a factor of 2 or 3) would be necessary to account for the observed decrease in Raman emission. Time-resolved Raman spectra with SSD (not presented here) are typically delayed by 100 to 200 ps relative to the Raman spectra without bandwidth. This time delay corresponds approximately to a two-times-higher laser pulse intensity at the onset of the Raman emission in the presence of SSD. A more accurate determination of the Raman threshold with SSD requires further experiments.

If the Raman emission were to occur on a density shelf resulting from profile steepening by the TPD instability, the threshold for Raman scattering would be

determined by the intensity required to produce a significant nonlinear level of TPD plasma waves, which should correspond roughly to the threshold for the TPD self-scattering. This is consistent with the non-SSD observations of the two thresholds (i.e., Raman and 3/2-harmonic self-scattering). However, the level of TPD plasma waves would determine the density of the shelf and would have to vary in such a way as to match the temporal fall-off of the Raman density in Fig. 51.5. The absence of strongly driven TPD during the late-time Raman emission of Fig. 51.5(c) indicates that neither the fast-electron model nor the density-shelf model may be applicable in this case.

Discussion

One notable result of this investigation is the apparent interconnection between the TPD and the Raman spectra. The time-resolved Raman data appear to indicate that in the presence of densities $>0.2\,n_c$ the Raman emission originates in regions of lower density. It is therefore possible that the presence of the TPD instability at $>0.2\,n_c$ excludes the Raman instability, perhaps through enhanced ion fluctuations, which are invariably observed to accompany the TPD instability.[37] Such enhanced ion fluctuations[38] have indeed been observed to suppress Raman scattering so that this conjecture would be self-consistent. The apparent preponderance of large-k_p plasmons may be related to the disappearance of the quarter-critical surface at $t \approx 1.5$ ns. For later times, the density hovers relatively close to the Landau cutoff density (see Fig. 51.5).

The apparent saturation observed at the highest intensities in Fig. 51.4 is probably a result of the rapid temporal evolution of the Raman spectra to the Landau cutoff rather than to any linear or nonlinear saturation effect. The time-resolved Raman spectra (Fig. 51.5) appear to furnish a possible explanation for this saturation. Since the SRS emission threshold lies near 2×10^{14} W/cm^2 and the Raman emission region drops in density rapidly to its Landau cutoff density, increasing the interaction beam intensity beyond a certain value will simply shift the Raman onset and cutoff toward earlier times without significantly changing the total Raman emission.

The strong decrease in Raman signal upon application of SSD bandwidth is consistent with observations elsewhere and is compatible with the inferred interconnection between the TPD and the Raman instabilities. Thus, the TPD instability would be only modestly affected by SSD through a two- to four-fold increase in its threshold, perhaps as a consequence of reduced filamentation, and hence reduced peak pump intensity driving the TPD instability. The same increase in the SRS threshold would lead to a very marked reduction in Raman signal because of its strong intensity scaling (see Fig. 51.4). Again, we note the alternative possibility that SSD can modify the Langmuir collapse of the TPD plasmons, leading to reduced fast-electron emission and a lower level of enhanced Raman scattering.

Our basic observations relating to the sensitivity of the TPD and SRS instabilities to SSD (or ISI) beam-smoothing techniques are consistent with observations made elsewhere at different wavelengths and under different plasma conditions.[17–20,31] However, the apparent interconnection between the

TPD and SRS instabilities has not been found in these references, possibly because no simultaneous 3/2-harmonic and Raman measurements were made.

Summary

We have successfully used the flexibility afforded by the multiple-beam OMEGA system to generate hot, long-scale-length plasmas and to study parametric instabilities at and below $n_c/4$ at an irradiation wavelength of 351 nm. The data indicate that the TPD instability extends all the way to its Landau cutoff at $n_e \approx 0.2\ n_c$. We have further shown that this instability is only modestly affected by beam-smoothing techniques such as SSD. It is possible that this last effect is a result of reduced filamentation of the interaction beam in the preformed plasma.

We have no evidence in our experiments that the Raman emission occurs at densities $\geq 0.2\ n_c$. In fact, it is observed only well below the TPD Landau cutoff density, typically at $n_e \leq 0.16\ n_c$. Furthermore, this emission rapidly chirps down to lower density (shorter wavelengths) until it reaches its Landau cutoff density, which can be used as an electron temperature diagnostic. Estimates of the latter agree with temperatures predicted by *SAGE*. Further, the Raman emission is strongly reduced upon the introduction of SSD. We have proposed a number of possible explanations for these observations but further experiments will be required to clarify remaining ambiguities.

ACKNOWLEDGMENT

The authors would like to thank the OMEGA operations group for their expert help in carrying out the complex experiments reported here. Special thanks are also owed to S. Noyes for fabricating the targets and to the experimental plasma physics group at Lawrence Livermore National Laboratory for the loan of the streak camera whose data were most essential to the success of the experiments reported here.

This work was supported by the U.S. Department of Energy Office of Inertial Confinement Fusion under agreement No. DE-FC03-85DP40200 and by the Laser Fusion Feasibility Project at the Laboratory for Laser Energetics, which is sponsored by the New York State Energy Research and Development Authority and the University of Rochester.

REFERENCES

1. W. Seka, R. S. Craxton, R. E. Bahr, D. L. Brown, D. K. Bradley, P. A. Jaanimagi, B. Yaakobi, and R. Epstein, Phys. Fluids B **4**, 432 (1992).
2. Y. Kato *et al.*, Phys. Rev. Lett. **53**, 1057 (1984).
3. See National Technical Information Service Document No. DOE/DP40200-65 [LLE Review **33**, 1 (1987)]. Copies may be ordered from the National Technical Information Service, Springfield, VA, 22161.
4. S. Skupsky, R. W. Short, T. Kessler, R. S. Craxton, S. Letzring, and J. M. Soures, J. Appl. Phys. **66**, 3456 (1989).
5. C. S. Liu and M. N. Rosenbluth, Phys. Fluids **19**, 967 (1976).
6. A. Simon, R. W. Short, E. A. Williams, and T. Dewandre, Phys. Fluids **26**, 3107 (1983).
7. J. L. Bobin *et al.*, Phys. Rev. Lett. **30**, 594 (1973); P. Lee *et al.*, Appl. Phys. Lett. **24**, 406 (1974); H. C. Pant *et al.*, Opt. Commun. **16**, 396 (1976).

8. A. I. Avrov *et al.*, Sov. Phys. JETP **43**, 507 (1977); V. Yu. Bychenkov *et al.*, Beitr. Plasmaphys. **23**, 331 (1983); R. L. Berger and L. V. Powers, Phys. Fluids **28**, 2895 (1985).

9. W. Seka, B. B. Afeyan, R. Boni, L. M. Goldman, R. W. Short, and K. Tanaka, Phys. Fluids **28**, 2570 (1985).

10. W. L. Kruer, *The Physics of Laser Plasma Interactions* (Addison-Wesley, Redwood City, CA, 1988), p. 83.

11. E. M. Epperlein, Phys. Rev. Lett. **65**, 2145 (1990); E. M. Epperlein and R. W. Short, submitted for publication to Phys. Fluids B. (APS-DPP 1991 invited talk).

12. Similar assumptions have been made by S. J. Karttunen, Laser Part. Beams **3**, 157 (1985); however, Karttunen's analysis does not lead to agreement with our observations.

13. A. M. Rubenchik and V. E. Zakharov, in *Handbook of Plasma Physics*, edited by M. N. Rosenbluth and R. Z. Sagdeev (Elsevier Science Publishers, New York, 1991), Vol. 3, p. 335; R. Z. Sagdeev *et al.*, Sov. Phys. JETP **55**, 74 (1982).

14. H. A. Baldis, J. C. Samson, and P. B. Corkum, Phys. Rev. Lett. **41**, 1719 (1978).

15. A. B. Langdon, B. F. Lasinski, and W. L. Kruer, Phys. Rev. Lett. **43**, 133 (1979).

16. S. E. Coe, T. Afshar-rad, and O. Willi, Opt. Commun. **73**, 299 (1989).

17. O. Willi *et al.*, Opt. Commun. **70**, 487 (1989).

18. S. E. Coe *et al.*, Europhys. Lett. **10**, 31 (1989).

19. O. Willi *et al.*, Phys. Fluids B **2**, 1318 (1990).

20. T. A. Peyser *et al.*, Phys. Fluids B **3**, 1479 (1991).

21. A. J. Schmitt, Phys. Fluids **31**, 3079 (1988); A. J. Schmitt, Phys. Fluids B **3**, 186 (1991).

22. F. Amiranoff *et al.*, Bull. Am. Phys. Soc. **30**, 1528 (1985).

23. N. G. Basov *et al.*, in *Proceedings on Basic and Advanced Diagnostic Techniques for Fusion Plasmas*, Varenna, Italy, 1986, edited by P. E. Stott *et al.* (Commission of European Communities, Directorate General XII, Brussels, 1986), Vol. 3, p. 997; and N. G. Basov *et al.*, Phys. Lett. **77A**, 163 (1980).

24. K. Tanaka, L. M. Goldman, W. Seka, M. C. Richardson, J. M. Soures, and E. A. Williams, Phys. Rev. Lett. **48**, 1179 (1982).

25. R. P. Drake *et al.*, Phys. Fluids B **1**, 2217 (1989); R. P. Drake *et al.*, Phys. Fluids B **1**, 1089 (1989); R. P. Drake *et al.*, Phys. Fluids **31**, 1795 (1988); R. P. Drake *et al.*, Phys. Rev. Lett. **60**, 1018 (1988).

26. A. V. Kil'pio *et al.*, Sov. J. Quantum Electron. **20**, 536 (1990).